The Chemistry of Vanadium−Carbon Bond Functionalities over an Oxo-Surface Defined by the Calix[4]arene Skeleton: The Redox Relationship between Vanadium(III) and Vanadium(IV) Assisted by Carbon−Oxygen Bond Cleavage

Barbara Castellano, Euro Solari, and Carlo Floriani*

Institut de Chimie Minérale et Analytique, BCH, Université de Lausanne, CH-1015 Lausanne, Switzerland

Nazzareno Re

Dipartimento di Chimica, Università di Perugia, I-06100 Perugia, Italy

Angiola Chiesi-Villa and Corrado Rizzoli

Dipartimento di Chimica, Università di Parma, I-43100 Parma, Italy

Received January 22, 1998

This report deals with the chemistry of V−C functionalities anchored to a quasi-planar O_4 matrix represented here by the [*p*-Bu^t-calix[4]-$(OMe)_2(O)_2$]$^{2-}$ macrocycle. The starting material [*p*-Bu^t-calix[4]-$(OMe)_2(O)_2$V−Cl], **2**, has been converted into the corresponding alkyl and aryl derivatives [*p*-Bu^t-calix[4]-$(OMe)_2(O)_2$V−R] (R = Me, **3**; R = CH_2Ph, **4**; R = *p*-MeC_6H_4, **5**) by conventional procedures. The structure of **5** reveals the self-assembling of the monomeric unit into a columnar arrangement with the *p*-tolyl substituent functioning as a guest moiety in a neighboring unit. Complexes **3**−**5** undergo migratory insertion reactions with CO and Bu^{t}NC to the corresponding η^2-acyls [*p*-Bu^t-calix[4]-$(OMe)_2(O)_2$V(η^2-COR)] (R = Me, **6**; R = CH_2Ph, **7**) and η^2-iminoacyls [*p*-Bu^t-calix[4]-$(OMe)_2(O)_2$V{η^2-C(NBu^t)R}] (R = Me, **8**; R = CH_2Ph, **9**; R = *p*-MeC_6H_4, **10**), the reaction with CO being strongly dependent on the R substituent. The structural model for the hexacoordinate intermediate leading to the inserted product is exemplified by the d^2 high-spin [*p*-Bu^t-calix-[4]-$(OMe)_2(O)_2$V(Cl)(CNBu^t], **11**, and proves the presence of four available orbitals at the metal for driving the reactivity in the [*p*-Bu^t-calix[4]-$(OMe)_2(O)_2$V] fragment. The bonding mode of the organic functionalities at the metal and the conversion of the alkyl substituent into the η^2-acyl have been inspected by extended Hückel calculations. The oxidative demethylation of **3** and **5** by a controlled amount of iodine opened an interesting synthetic route to the corresponding vanadium(IV) organometallic derivatives [*p*-Bu^t-calix[4]-(OMe)-$(O)_3$V−X] (X = Cl, **12**; X = *p*-MeC_6H_4, **13**). A structural report on **2**, **5**, and **9** is included.

Introduction

The calix[4]arene skeleton[1] provides a unique preorganized O_4 quasi-planar environment for organometallic functionalities[2] which can, in turn, be adapted to the oxidation state and the required degree of functionalization of the metal via the appropriate alkylation of the phenoxo oxygens. Although the oxygen atom environment is common in vanadium chemistry,[3] it is rarely used to support the V−C functionality.[4] It is also surprising that the rich organometallic chemistry of niobium and tantalum,[5] based on alkoxo and phenoxo ligands, is not mirrored for vanadium. In light of these comments, it is appropriate that we draw attention to the recent impact that silica-supported vanadium catalysts have had in olefin polymerization[6] and to the

* To whom correspondence should be addressed.

(1) (a) Gutsche, C. D. *Calixarenes*; The Royal Society of Chemistry: Cambridge, U.K., 1989. (b) *Calixarenes, A Versatile Class of Macrocyclic Compounds*; Vicens, J. Böhmer, V., Eds.; Kluwer: Dordrecht, The Netherlands, 1991.

(2) (a) Giannini, L.; Solari, E.; Floriani, C.; Chiesi-Villa, A.; Rizzoli, C. *J. Am. Chem. Soc.* **1998**, *120*, 823−824. (b) Zanotti-Gerosa, A.; Solari, E.; Giannini, L.; Floriani, C.; Chiesi-Villa, A.; Rizzoli, C. *J. Am. Chem. Soc.* **1998**, *120*, 437. (c) Giannini, L.; Caselli, A.; Solari, E.; Floriani, C.; Chiesi-Villa, A.; Rizzoli, C.; Re, N.; Sgamellotti, A. *J. Am. Chem. Soc.* **1997**, *119*, 9198. (d) *Ibid.* **1997**, *119*, 9709. (e) Caselli, A.; Giannini, L.; Solari, E.; Floriani, C.; Re, N.; Chiesi-Villa, A.; Rizzoli, C. *Organometallics* **1997**, *16*, 5457. (f) Giannini, L.; Solari, E.; Zanotti-Gerosa, A.; Floriani, C.; Chiesi-Villa, A.; Rizzoli, C. *Angew. Chem., Int. Ed. Engl.* **1997**, *36*, 753. (g) Giannini, L.; Solari, E.; Zanotti-Gerosa, A.; Floriani, C.; Chiesi-Villa, A.; Rizzoli, C. *Angew. Chem., Int. Ed. Engl.* **1996**, *35*, 2825. (h) Castellano, B.; Zanotti-Gerosa, A.; Solari, E.; Floriani, C.; Chiesi-Villa, A.; Rizzoli, C. *Organometallics* **1996**, *15*, 4894. (i) Giannini, L.; Solari, E.; Zanotti-Gerosa, A.; Floriani, C.; Chiesi-Villa, A.; Rizzoli, C. *Angew. Chem., Int. Ed. Engl.* **1996**, *35*, 85. (j) Gardiner, M. G.; Lawrence, S. M.; Raston, C. L.; Skelton, B. W.; White, A. H. *Chem. Commun.* **1996**, 2491. (k) Gardiner, M. G.; Koutsantonis, G. A.; Lawrence, S. M.; Nichols, P. J.; Raston, C. L. *Chem. Commun.* **1996**, 2035. (l) Gibson, V. C.; Redshaw, C.; Clegg, W.; Elsegood, M. R. J. *J. Chem. Soc., Chem. Commun.* **1995**, 2371. (m) Acho, J. A.; Doerrer, L. H.; Lippard, S. J. *Inorg. Chem.* **1995**, *34*, 2542.

S0276-7333(98)00038-7 CCC: $15.00
Publication on Web 05/02/1998

pioneering work of Feher who used silasesquioxanes as ancillary ligands to better understand the nature of the active silica-supported vanadium species.[7] An interesting relationship between the use of calix[4]arene as an ancillary ligand and other oxygen-supported organometallic functionalities has been found.[8] The purpose of this paper is, therefore, to report the genesis and reactivity of the V−C functionality anchored to the dimethoxy-*p*-*tert*-butylcalix[4]arene dianion (**A**) and the oxidative demethylation of the ligand as an entry into the analogous vanadium(IV) organometallic chemistry.

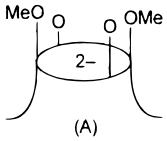

(A)

The extended Hückel calculations allowed us to define the frontier orbitals of the [calix[4]-$(OMe)_2(O)_2$V] fragment engaged in the transformation of the V−C bonds and into the conversion of vanadium(III) to vanadium(IV) organometallics.

Experimental Section

General Procedure. All reactions were carried out under an atmosphere of purified nitrogen. Solvents were dried and distilled before use by standard methods. ^{1}H NMR and IR spectra were recorded on Bruker AC-200 and DPX-400 and Perkin-Elmer FT 1600 instruments, respectively. GC and GC-MS analyses were carried out using a HP 5890 Series II system and a HP 5890A GC system, respectively. The magnetic measurements were carried out using a SQUID Quantum Design magnetometer. The syntheses of [*p*-Bu^t-calix[4]-$(OMe)_2$-$(OH)_2$], **1**,[9] and VCl_3·THF_3[10] were performed as reported in the literature.

Synthesis of 2. A *n*-hexane solution of BuLi (48.8 mL, 90.7 mmol) was added dropwise to a THF suspension (260 mL) of **1** (30.8 g, 45.4 mmol). The orange solution was then added dropwise to a violet THF suspension (260 mL) of $VCl_3(THF)_3$ (17.2 g, 46.0 mmol). After the mixture was stirred for 8 h, the suspension was evaporated to dryness and the green solid residue extracted with benzene (50 mL) and *n*-hexane (250 mL). The product was then collected (30.2 g, 87%). Anal. Calcd for **2**, $C_{46}H_{58}ClO_4V$: C, 72.55; H, 7.68. Found: C, 72.91; H, 7.69. Crystals were grown in toluene. $\mu_{eff} = 2.69\ \mu_B$ at 300 K.

Synthesis of 3. A diethyl ether solution of MeLi (6.50 mL, 11.52 mmol) was added dropwise to a benzene suspension (200 mL) of **2** (8.77 g, 11.52 mmol). After the mixture was stirred for 12 h, a dark suspension formed, which was then evaporated to dryness. The solid residue was extracted with diethyl ether. The solvent was removed in vacuo, and the residue was kept in *n*-hexane (60 mL) at 9 °C for 24 h and then collected as a violet powder (4.80 g, 51%). Anal. Calcd for **3**·Et_2O, $C_{51}H_{71}O_5V$: C, 75.14; H, 8.80. Found: C, 74.77; H, 8.48.

Synthesis of 4. A THF solution of $(PhCH_2)_2Mg$ (18.65 mL, 5.0 mmol) was added dropwise to a benzene suspension (200 mL) of **2** (7.67 g, 10.0 mmol). After the mixture was stirred for 4 h, a green solution formed. Dioxane (3 mL) was added, and after 2 h the suspension was filtered. The solvent was removed in vacuo, and the residue was kept in hexane (60 mL) at 9 °C for 24 h and finally collected (5.37 g, 66%). Anal. Calcd for **4**, $C_{53}H_{65}O_4V$: C, 77.90; H, 8.03. Found: C, 77.48; H, 8.13. $\mu_{eff} = 2.60\ \mu_B$ at 300 K.

Synthesis of 5. To a stirred benzene suspension (200 mL) of **2** (7.80 g, 10.24 mmol) was added dropwise a THF solution of *p*-MeC_6H_4MgBr (21.3 mL, 10.24 mmol). Stirring for 4 h resulted in a green solution. Dioxane (3 mL) was added, and after 2 h, the suspension was filtered. The solvent was removed in vacuo, and the residue was kept in hexane (60 mL) at 9 °C for 24 h and then collected (6.45 g, 77%). Anal. Calcd for **5**, $C_{53}H_{65}O_4V$: C, 77.90; H, 8.03. Found: C, 77.55; H, 8.10. Green crystals were grown in a saturated THF/benzene solution at room temperature.

Synthesis of 6. A benzene (200 mL) solution of **3**·Et_2O (2.86 g, 3.51 mmol) was saturated with CO, resulting in the solution turning red within seconds. After the mixture was stirred for 24 h, the solvent was removed and the residue washed with *n*-hexane (60 mL) and then collected as a red microcrystalline solid (1.60 g, 59%). Anal. Calcd for **6**, $C_{48}H_{61}O_5V$: C, 74.98; H, 7.99. Found: C, 74.96; H, 8.01. IR (Nujol, ν_{max}/cm^{-1}): 1599.3 (w), 1581.8 (m).

Synthesis of 7. A green benzene (100 mL) solution of **4** (2.78 g, 3.40 mmol) was saturated with CO at room temperature. The solution turned red within 1 h and was then kept stirring overnight. The solvent was removed, and the remaining solid residue was kept in hexane (60 mL) at 9 °C for 24 h and then collected as a dark red powder (2.0 g, 70%). Anal. Calcd for **7**, $C_{54}H_{65}O_5V$: C, 76.74; H, 7.78. Found: C, 76.72; H, 8.70. IR (Nujol, ν_{max}/cm^{-1}): 1599.7 (m), 1571.9 (s). $\mu_{eff} = 2.68\ \mu_B$ at 300 K.

Synthesis of 8. A benzene (30 mL) solution of Bu^{t}NC (0.221 g, 2.66 mmol) was added dropwise to a green benzene solution (80 mL) of **3**·Et_2O (2.17 g, 2.66 mmol) and the resulting dark yellow solution was stirred overnight. The solvent was evaporated to dryness and the residue was kept

(3) (a) Vilas Boas, L. F.; Costa Pessoa, J. In *Comprehensive Coordination Chemistry*; Wilkinson, G., Gillard, R. D., McCleverty, J. A., Eds.; Pergamon: Oxford, 1987; Vol. 3, Chapter 33, p 453. (b) *Vanadium in Biological Systems*; Chasteen, N. D. Ed.; Kluwer: Dordrecht, The Netherlands, 1990. (c) Mazzanti, M.; Floriani, C.; Chiesi-Villa, A.; Guastini, C. *J. Chem. Soc., Dalton Trans.* **1989**, 1793. (d) Mazzanti, M.; Floriani, C.; Chiesi-Villa, A.; Guastini, C. *Angew. Chem., Int. Ed. Engl.* **1988**, *27*, 576.

(4) Seidel, W.; Kreisel, G. *Z. Chem.* **1981**, *21*, 295. Preuss, F.; Ogger, L. *Z. Naturforsch.* **1982**, *37b*, 957. Seangprasertkij, R.; Riechel, T. L. *Inorg. Chem.* **1986**, *25*, 3121. Preuss, F.; Becker H. *Z. Naturforsch.* **1986**, *41b*, 185.

(5) Parkin, B. C.; Clark, J. R.; Visciglio, V. M.; Fanwick, P. E.; Rothwell, I. P. *Organometallics* **1995**, *14*, 3002. Clark, J. R.; Fanwick, P. E.; Rothwell, I. P. *J. Chem. Soc., Chem. Commun.* **1995**, 553. Yu, J. S.; Ankianiec, B. C.; Rothwell, I. P.; Nguyen, M. T. *J. Am. Chem. Soc.* **1992**, *114*, 1927. Chesnut, R. W.; Jacob, G. G.; Yu, J. S.; Fanwick, P. E.; Rothwell, I. P. *Organometallics* **1991**, *10*, 321. Bonanno, J. B.; Lobkovsky, E. B.; Wolczanski, P. T. *J. Am. Chem. Soc.* **1994**, *116*, 11159. Miller, R. L.; Toreki, R.; LaPointe, R. E.; Wolczanski, P. T.; Van Duyne, G. D.; Roe, D. C. *J. Am. Chem. Soc.* **1993**, *115*, 5570. Wigley, D. E.; Gray, S. D. In *Comprehensive Organometallic Chemistry II*; Abel, E. W., Stone, F. G. A., Wilkinson, G., Eds.; Pergamon: Oxford, 1995; Vol. 5, Chapter 2, pp 57−153.

(6) Karol, F. J.; Cann, K. J.; Wagner, B. E. In *Transition Metals and Organometallics as Catalysts for Olefin Polymerization*; Kaminsky, W., Sinn, H., Eds.; Springer: New York, 1988; pp 149−161.

(7) Feher, F. J.; Newman, D. A.; Walzer, J. F. *J. Am. Chem. Soc.* **1989**, *111*, 1741. Feher, F. J.; Walzer, J. F. *Inorg. Chem.* **1991**, *30*, 1689. Feher, F. J.; Walzer, J. F.; Blanski, R. L. *J. Am. Chem. Soc.* **1991**, *113*, 3618. Feher, F. J.; Blanski, R. L. *J. Am. Chem. Soc.* **1992**, *114*, 5886. Feher, F. J.; Blanski, R. L. *Organometallics* **1993**, *12*, 958. Feher, F. J.; Budzichowski, T. A. *Polyhedron* **1995**, *14*, 3239 and references therein.

(8) For related molecular approaches to oxo-surfaces binding organometallic functionalities see: Chisholm, M. H. *Chemtracts-Inorg. Chem.* **1992**, *4*, 273. Kläui, W. *Angew. Chem., Int. Ed. Engl.* **1990**×e*229*, 627. Feher, F. J.; Budzichowski, T. A. *Polyhedron* **1995**, *14*, 3239. Nagata, T.; Pohl, M.; Weiner, H.; Finke, R. G. *Inorg. Chem.* **1997**, *36*, 1366. Pohl, M.; Lyon, D. K.; Mizuno, N.; Nomiya, K.; Finke, R. G. *Inorg. Chem.* **1995**, *34*, 1413. Corker, J.; Lefebvre, F.; Lecuyer, C.; Dufaud, V.; Quignard, F.; Choplin, A.; Evans, J.; Basset, J.-M. *Science* **1996**, *271*, 966. Niccolai, G. P.; Basset, J.-M. *Appl. Catal., A* **1996**, *146*, 145. Vidal, V.; Theolier, A.; Thivolle-Cazat, J.; Basset, J.-M.; Corker, J. *J. Am. Chem. Soc.* **1996**, *118*, 4595. *Mechanisms of Reactions of Organometallic Compounds with Surfaces*; Cole-Hamilton, D. J., Williams, J. O., Eds.; Plenum: New York, 1989.

(9) Arduini, A.; Casnati, A. In *Macrocycle Synthesis*; Parker, O., Ed.; Oxford University Press: New York, 1996; Chapter 7.

(10) Manzer, L. E. *Inorg. Synth.* **1982**, *21*, 135.

in *n*-hexane (60 mL) at 9 °C for 24 h and finally collected as a yellow microcrystalline solid (1.42 g, 53%). Anal. Calcd for **8**·C_6H_{14}, $C_{52}H_{70}NO_4V$·C_6H_{14}, $C_{58}H_{84}NO_4V$: C, 76.52; H, 9.32; N, 1.54. Found: C, 76.36; H, 9.00; N, 1.30. IR (Nujol, ν_{max}/cm^{-1}): 1613.7 (w), 1599.1 (m).

Synthesis of 9. A benzene (20 mL) solution of Bu^{t}NC (0.30 g, 3.72 mmol) was added dropwise to a benzene solution (80 mL) of **4** (3.04 g, 3.72 mmol) and the resulting dark orange solution was stirred overnight. The solvent was evaporated to dryness, and the residue was washed with *n*-hexane (60 mL), kept in *n*-hexane at 9 °C for 24 h, and finally collected as an orange microcrystalline solid (2.65 g, 79%). Crystals were grown in a mixture (1/1) of hexane−benzene. Anal. Calcd for **9**, $C_{58}H_{74}NO_4V$: C, 77.37; H, 8.30; N, 1.55. Found: C, 77.14; H, 8.24; N, 1.27. IR (Nujol, ν_{max}/cm^{-1}): 1625.6 (s), 1598.1 (s). $\mu_{eff} = 2.75\ \mu_B$ at 300 K.

Synthesis of 10. A benzene (30 mL) solution of Bu^{t}NC (0.20 g, 2.45 mmol) was added dropwise to a benzene solution (80 mL) of **5** (2.00 g, 2.45 mmol), and the resulting dark green solution was stirred overnight. The solvent was removed, and the remaining residue was kept in *n*-hexane (60 mL) at 9 °C for 24 h and finally collected as a green powder (1.76 g, 73%). Anal. Calcd for **10**·C_6H_{14}, $C_{64}H_{88}NO_4V$: C, 77.93; H, 9.01; N, 1.42. Found: C, 78.07; H, 8.87; N, 1.24. IR (Nujol, ν_{max}/cm^{-1}): 1614.5 (s), 1597.6 (s).

Synthesis of 11. Bu^{t}NC (0.248 g, 2.98 mmol) was added to a stirred red THF (120 mL) solution of **2** (2.26 g, 2.98 mmol). After 12 h, the solvent was removed and the remaining residue washed with pentane (60 mL) and collected as a green powder (2.0 g, 73%). Anal. Calcd for **11**·THF, $C_{55}H_{75}ClNO_5V$: C, 72.06; H, 8.26; N, 1.53. Found: C, 72.04; H, 8.69; N, 1.17. IR (Nujol, ν_{max}/cm^{-1}): 2194.3 (m), 1589.9 (w). $\mu_{eff} = 2.67\ \mu_B$ at 300 K.

Synthesis of 12. A THF (20 mL) solution of I_2 (0.24 g, 1.0 mmol) was added dropwise to a cooled (−30 °C) THF red solution (120 mL) of **2** (1.60 g, 2.10 mmol). After the mixture was stirred for 12 h at room temperature, the solvent was removed in vacuo and the red residue washed with pentane (60 mL) and collected (1.2 g, 70%). Anal. Calcd for **12**·THF, $C_{49}H_{63}ClO_5V$: C, 71.90; H, 7.76. Found: C, 71.51; H, 7.33. A sample of **12** in C_6D_6 was hydrolyzed by diffusion of aqueous HCl under N_2. *p*-Bu^t-calix[4]-(OMe)$(OH)_3$ was identified in the ^{1}H NMR spectrum. A sample of the crude reaction product was analyzed by CG-MS: CH_3I was identified. ^{1}H NMR of the hydrolyzed product (C_6D_6, 298 K, ppm): δ 9.93 (s, 1H, OH), 9.69 (s, 2H, OH), 7.00 (m, 8H, arom), 4.50 (d, 2H, J = 13.8 Hz, CH_2-calix), 4.38 (d, 2H, J = 13.8 Hz, CH_2-calix), 3.54 (s, 3H, OCH_3-calix), 3.42 (d, 2H, J = 13.8 Hz, CH_2-calix), 3.31 (d, 2H, J = 13.8 Hz, CH_2-calix), 1.27 (s, 18H, Bu^t-calix), 0.97 (s, 9H, Bu^t-calix), 0.89 (s, 9H, Bu^t-calix).

Synthesis of 13. A THF solution of I_2 (0.32 g, 1.265 mmol) was added dropwise to a cooled (−30 °C) THF suspension (150 mL) of **5** (2.06 g, 2.53 mmol). The solution became red within seconds. Stirring was continued for 12 h at room temperature. The red solution was filtered, the solvent removed in vacuo, and the red residue finally washed with *n*-hexane (80 mL) and collected (2.0 g, 94%). Anal. Calcd for **13**·0.5C_6H_{14}, $C_{55}H_{69}O_4V$: C, 78.15; H, 8.25. Found: C, 77.60; H, 8.55. Crystals were grown in hexane solution at room temperature. A sample of **13** in C_6D_6 was hydrolyzed by diffusion of aqueous HCl under N_2. *p*-Bu^t-calix[4]-(OMe)$(OH)_3$ was identified in the ^{1}H NMR spectrum. A sample of the crude reaction product was analyzed by CG-MS: CH_3I was identified. For the ^{1}H NMR of the hydrolyzed product, see preceding preparation. $\mu_{eff} = 1.65\ \mu_B$ at 300 K.

Synthesis of 14. A THF (20 mL) solution of I_2 (0.29 g, 1.14 mmol) was added dropwise to a stirred THF solution (120 mL) of **13**·0.5C_6H_{14} (0.968 g, 1.14 mmol) at room temperature. After the mixture was stirred for 12 h, the solvent was removed in vacuo and the red residue extracted with *n*-hexane (150 mL). The complex was obtained as black crystals from this solution (0.65 g, 74%). Anal. Calcd for **14**·2C_4H_8O, $C_{96}H_{120}O_{10}V_2$: C, 75.02; H, 7.89. Found: C, 75.28; H, 8.67. A sample of the crude reaction product was analyzed by CG-MS: CH_3I and *p*-iodotoluene were identified.

X-ray Crystallography for Complexes 2, 5, and 9. Suitable crystals were mounted in glass capillaries and sealed under nitrogen. The reduced cells were obtained with the use of TRACER.[11] Crystal data and details associated with data collection are given in Tables 1 and S1 (Supporting Information). Data were collected on a single-crystal diffractometer (Siemens AED for **2** and Rigaku AFC6S for **5** and **9**) at 295 K for **2** and **5** and 133 K for **9**. For intensities and background, the individual reflection profiles were analyzed.[12] The structure amplitudes were obtained after the usual Lorentz and polarization corrections, and the absolute scale was established by the Wilson method.[13] The crystal quality was tested by ψ scans, showing that crystal absorption effects could not be neglected. Data for all complexes were then corrected for absorption using ABSORB[14] for **2** and a semiempirical method[15] for **5** and **9**. The function minimized during the full-matrix least-squares refinements was $\sum w(\Delta F^2)^2$. Anomalous scattering corrections were included in all structure factor calculations.[16b] Scattering factors for neutral atoms were taken from ref 16a for non-hydrogen atoms and from ref 17 for H. Structure solutions[18] were based on the observed reflections [$I > 2\sigma(I)$], while the refinements were based on the unique reflections having $I > 0$.[19] The structures were solved by the heavy-atom method starting from a three-dimensional Patterson map. Refinements were done by full-matrix least-squares, first isotropically and then anisotropically for all non-H atoms except for the disordered atoms. For all complexes, the hydrogen atoms were located in a difference Fourier map and introduced in the refinements as fixed atom contributions (U_{iso} = 0.10 Å^2 for **2** and **5** and 0.05 Å^2 for **9**). The H atoms associated to the disordered carbon atoms were ignored as well as the H atoms of the C55 methyl group in complex **5**, which are required to be statistically distributed over two positions. In the last stage of refinement, the weighting scheme $w = 1/[\sigma^2(F_o^2) + (aP)^2]$ (with $P = (F_o^2 + 2F_c^2)/3$ was applied with a having values of 0.1204, 0.1220, and 0.1169 for **2**, **5**, and **9**, respectively. All calculations were performed using SHELX92. The final difference maps showed no unusual features, with no significant peaks above the general background.

In complex **2**, all of the methyl carbon atoms of the *tert*-butyl groups of calixarene showed high thermal parameters, indicating the presence of disorder. The atoms were then split over two positions (called A and B) isotropically refined with site occupation factors of 0.5. In complexes **5** and **9**, the methyl carbon atoms of the *tert*-butyl group (C30, C31, C32 for **5**; C34, C35, C36 for **9**) were found to be disordered over two positions (called A and B) and isotropically refined with site occupation factors of 0.6 and 0.4, respectively. Moreover, the benzene solvent molecule of crystallization in complex **5** was found to be distributed over two positions (A and B) and was isotropically refined with a site occupation factor of 0.5, constraining the aromatic ring to have a D_{6h} symmetry.

(11) Lawton, S. L.; Jacobson, R. A. *TRACER (a cell reduction program)*; Ames Laboratory, Iowa State University of Science and Technology: Ames, IA, 1965.
(12) Lehmann, M. S.; Larsen, F. K. *Acta Crystallogr., Sect. A: Cryst. Phys., Diffr., Theor. Gen. Crystallogr.* **1974**, *A30*, 580−584.
(13) Wilson, A. J. C. *Nature* **1942**, *150*, 151.
(14) Ugozzoli, F. *Comput. Chem.* **1987**, *11*, 109.
(15) North, A. C. T.; Phillips, D. C.; Mathews, F. S. *Acta Crystallogr., Sect. A: Cryst. Phys., Diffr., Theor. Gen. Crystallogr.* **1968**, *A24*, 351.
(16) (a) *International Tables for X-ray Crystallography*; Kynoch Press: Birmingham, England, 1974; Vol. IV, p 99. (b) *Ibid.* p 149.
(17) Stewart, R. F.; Davidson, E. R.; Simpson, W. T. *J. Chem. Phys.* **1965**, *42*, 3175.
(18) Sheldrick, G. M. *SHELX76. Program for crystal structure determination.* University of Cambridge: England, 1976.
(19) Sheldrick, G. M. *SHELXL92. Program for Crystal Structure Refinement*. University of Göttingen: Göttingen, Germany, 1992.

Table 1. Experimental Data for the X-ray Diffraction Studies on Complexes 2, 5, and 9

	2	5	9
formula	$C_{46}H_{58}ClO_4V\cdot C_7H_8$	$C_{53}H_{65}O_4V\cdot{}_2C_6H_6$	$C_{58}H_{74}NO_4V\cdot 3.5C_6H_6$
a, Å	17.523(3)	24.019(5)	14.587(3)
b, Å	13.479(2)	10.837(2)	17.769(4)
c, Å	21.676(3)	24.130(4)	14.329(4)
α, °	90	90	103.24(2)
β, °	108.10(2)	110.74(1)	106.44(2)
γ, °	90	90	72.59(2)
V, Å^3	4866.4(14)	5873.9(19)	3356.4(15)
Z	4	4	2
fw	853.5	973.3	1173.6
space group	$P2_1/c$ (No. 14)	$C2/c$ (No. 15)	$P\bar{1}$ (No. 2)
T, °C	295	295	143
λ, Å	1.54178	1.54178	1.54178
ρ_{calc}, g cm^{-3}	1.165	1.101	1.161
μ, cm^{-1}	25.43	17.38	16.02
transmission coeff	0.827−1.000	0.742−1.000	0.456−1.000
no. of unique data used in refinement [$I > 0$] (NO)	7386	4223	6302
no. of unique obsd data [$I > 2\sigma(I)$]	3248	1654	3772
no. of params refined (NV)	520	285	758
overdetermn ratio (NO/NV)	14.2	14.8	8.3
R[a]	0.068	0.074	0.064
wR2[b]	0.189	0.243	0.191

[a] $R = \sum|\Delta F| / \sum|F_o|$ calculated on the unique observed data [$I > 2\sigma(I)$]. [b] $wR2 = [\sum w|\Delta F^2|^2/\sum w|F_o^2|^2]^{1/2}$ calculated on the unique data with $I > 0$.

Table 2. Selected Bond Distances (Å) and Angles (deg) for Complexes 2, 5, and 9

	2	5	9
V(1)−X[a]	2.265(2)	2.042(10)	2.047(8)
V(1)−N(1)			2.050(7)
V(1)−O(1)	1.809(4)	1.841(5)	1.883(5)
V(1)−O(2)	2.156(4)	2.137(4)	2.179(4)
V(1)−O(3)	1.805(4)		1.860(4)
V(1)−O(4)	2.128(4)		2.161(3)
O(1)−C(1)	1.329(6)	1.344(9)	1.314(8)
O(2)−C(13)	1.419(6)	1.425(6)	1.395(9)
O(2)−C(45)	1.443(6)	1.447(8)	1.450(6)
O(3)−C(20)	1.353(7)		1.309(6)
O(4)−C(27)	1.417(5)		1.419(8)
O(4)−C(46)	1.455(6)		1.452(9)
N(1)−C(51)			1.266(8)
N(1)−C(59)			1.501(10)
C(51)−C(52)			1.495(10)
O(2)−V(1)−O(4)[b]	167.5(1)	167.6(1)	164.1(2)
O(1)−V(1)−O(3)	127.3(2)	139.0(2)	113.9(2)
X−V(1)−O(3)	117.8(1)	110.5(1)	136.0(2)
X−V(1)−O(1)	114.9(1)	110.5(1)	110.0(2)
X−V(1)−N(1)			36.0(3)
V(1)−O(1)−C(1)	167.3(4)	153.1(4)	159.9(4)
V(1)−O(2)−C(45)	131.3(3)	128.5(4)	130.3(4)
V(1)−O(2)−C(13)	114.6(3)	117.4(4)	116.8(4)
C(13)−O(2)−C(45)	114.1(4)	114.1(4)	112.7(5)
V(1)−O(3)−C(20)	161.7(4)		169.1(4)
V(1)−O(4)−C(46)	128.6(3)		127.0(4)
V(1)−O(4)−C(27)	118.7(3)		119.1(3)
C(27)−O(4)−C(46)	112.7(3)		113.6(5)
V(1)−N(1)−C(59)			154.7(5)
V(1)−N(1)−X			71.9(4)
X−N(1)−C(59)			133.1(7)
V(1)−X−N(1)			72.1(5)
N(1)−X−C(52)			129.6(7)
V(1)−X−C(52)			157.9(5)

[a] X should be read Cl(1) for complex **2** and C(51) for complexes **5** and **9**. [b] In complex **5**, O(3) and O(4) should be read O(1)′ and O(2)′, respectively (prime (′) = $-x$, y, $0.5 - z$).

Final atomic coordinates are listed in Tables S2−S4 (Supporting Information) for non-H atoms and in Tables S5−S7 (Supporting Information) for hydrogens. Thermal parameters are given in Tables S8−S10 (Supporting Information), and bond distances and angles are given in in Tables S11−S13 (Supporting Information).[20]

(20) See paragraph at the end regarding Supporting Information.

Table 3. Comparison of Relevant Conformational Parameters within Calixarene for Complexes 2, 5, and 9

	2	5	9
(a) Dihedral Angles (deg) between Planar Moieties[a]			
E ∧ **A**	139.0(1)	132.4(2)	133.9(1)
E ∧ **B**	109.7(1)	112.9(2)	111.5(1)
E ∧ **C**	138.5(1)	132.4(2)	148.9(2)
E ∧ **D**	117.8(1)	112.9(2)	113.5(2)
A ∧ **C**	97.5(2)	95.2(2)	95.9(2)
B ∧ **D**	132.5(1)	134.3(2)	134.9(2)
(b) Contact Distances (Å) between *para*-Carbon Atoms of Opposite Aromatic Rings[b]			
C4...C17	9.453(9)	9.057(11)	9.357(9)
C10...C24	7.473(6)	7.446(9)	7.386(9)

[a] **E** (reference plane) refers to the least-squares mean plane defined by the C(7), C(14), C(21), C(28) bridging methylenic carbons. **A**, **B**, **C**, and **D** refer to the least-squares mean planes defined by the aromatic rings bonded to O(1), O(2), O(3), and O(4), respectively. In complex **5**, O(3), O(4), C(21), and C(28) should be read O(1)′, O(2)′, C(7)′, and C(14)′, respectively (prime (′) = $-x$, y, $0.5 - z$). [b] In complex **5**, C(17) and C(24) should be read C(4)′ and C(10)′, respectively (prime (′) = $-x$, y, $0.5 - z$).

Results and Discussion

The parent compound **2** can be considered a useful entry point into the organometallic chemistry of vanadium bonded to the oxo-matrix defined by the calix[4]-arene skeleton. It was prepared by reacting **1**, pretreated with BuLi, with $VCl_3\cdot THF_3$. Complex **2** is a yellow-green crystalline solid with the paramagnetism expected for a d^2 high-spin complex ($\mu_{eff} = 2.69\ \mu_B$ at 300 K).

A selection of bond distances and angles for complexes **2**, **5**, and **9** is given in Table 2. Structural parameters concerning the conformation of the [calix[4]arene-(OMe_2)V] units are compared in Table 3. The aromatic rings bonded to the O(1), O(2), O(3), and O(4) oxygen atoms are labeled A, B, C, and D, respectively.

The structure of complex **2** is shown in Figure 1. Vanadium has a pseudo-trigonal-bipyramidal coordina-

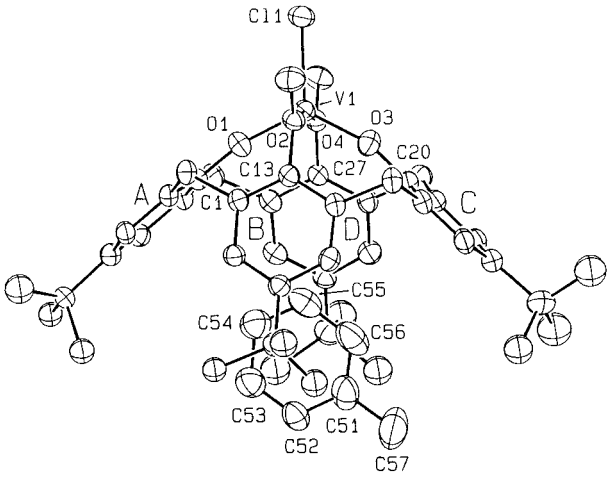

Figure 1. ORTEP drawing of complex **2** (30% probability ellipsoids). Disorder has been omitted for clarity.

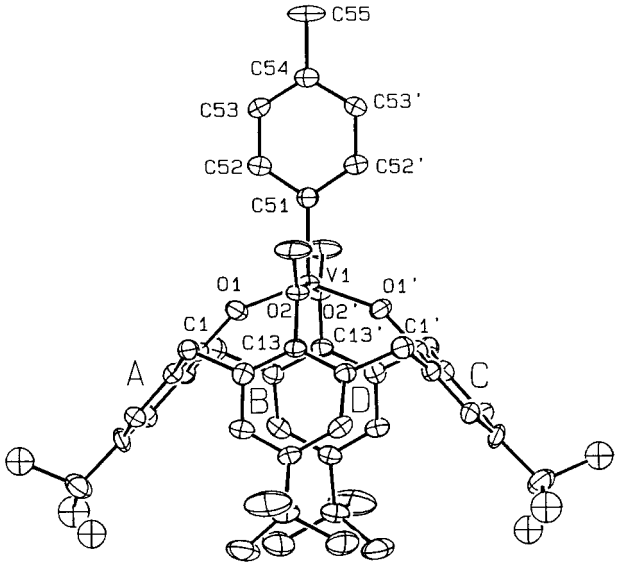

Figure 2. ORTEP drawing of complex **5** (30% probability ellipsoids). Prime denotes a transformation of $-x, y, 0.5 - z$. Disorder has been omitted for clarity.

tion environment with the equatorial plane being defined by V, Cl, O(1), O(3). The V−O bond distances vary from 1.807(2) (mean value for V−O(1) and V−O(3)) to 2.142(14) Å (mean value for V−O(2) and V−O(4)), the latter being related to the methoxy groups. The V−O(1) and V−O(3) bond distances along with the values of the V−O(1)−C(1) (167.3(4)°) and V−O(3)−C(21) (161.7(4)°) bond angles are in agreement with a V−O multiple bond.[3c,d] Because of the presence of the methoxy groups, the O_4 core is tetrahedrally distorted (distortion ranging from −0.349(4) to 0.224(3) Å; vanadium protrudes by 0.453(1) Å), resulting in an elliptical cross section conformation of the macrocycle elongated along the O(1)···O(3) direction as is observed from the dihedral angles and the contact distances quoted in Table 3. This conformation allows the aromatic ring of a toluene molecule of crystallization to enter as a guest nearly parallel to the O(1),V,O(3) direction (dihedral angle 10.2-(2)°) and perpendicular to the C(1)···C(6) and C(15)···C-(20) rings (dihedral angles 87.7(2)° and 82.5(2)°, respectively) with the C(55)−H(55) bond directly below the vanadium atom (V···C(55) 4.614(8) Å; V···H(55)−C(55) 166.5°).

Scheme 1

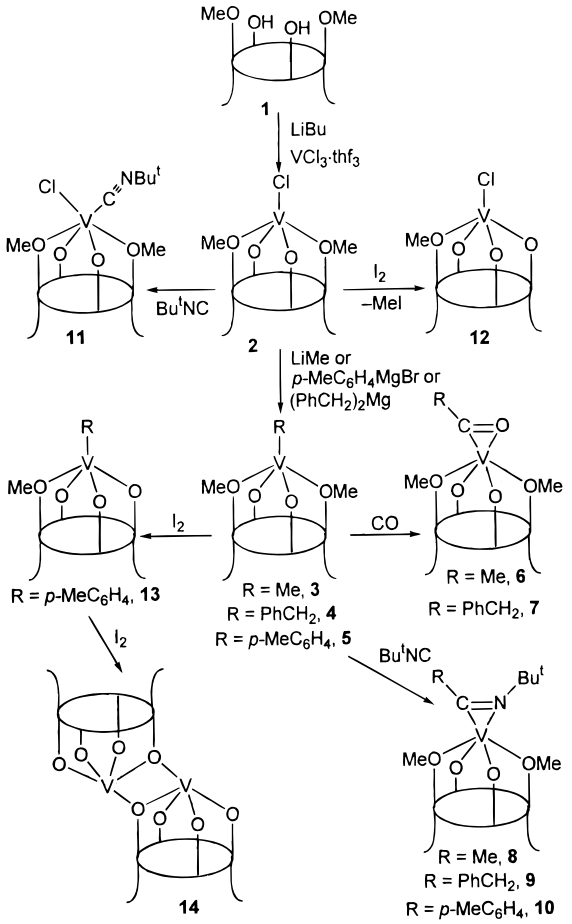

Complex **2** undergoes alkylation to the corresponding paramagnetic vanadium(III) derivatives **3**−**5** using either a lithium or a Grignard reagent as described in the Experimental Section (Scheme 1). They have been isolated as thermally stable organometallic derivatives, although they undergo facile oxidative transformations (see below). The proposed structure for **3**−**5** is supported by the X-ray analysis of **5**, which additionally showed a particularly interesting solid-state self-assembling of the organometallic monomeric unit.

Complex **5** possesses a crystallographically imposed C_2 symmetry, the 2-fold axis running through the molecular axis (see Figure 2). The main feature of the solid-state structure consists of the packing of the molecules along the 2-fold axis: each complex molecule includes the *p*-tolyl ligand of an adjacent molecule translated along the *b* crystallographic axis and positioned with the methyl group (C(55)) directly below the vanadium atom at a separation of 4.380(10) Å. This results in a head-to-tail columnar chain arrangement of the molecules running along the 2-fold axis (Figure 3). The arrangement is very close to that observed in an analogous Ti derivative.[21] The host−guest interactions could be interpreted in terms of CH_3/π interactions between the protons of the C(55) methyl group of the guest and the symmetry-related C(8)···C(13) and C(8′)···C(13′) aromatic rings (′ = $-x, y, 0.5 - z$). The rather narrow range of the C_{methyl}···C_{ring} separations

(21) Zanotti-Gerosa, A.; Solari, E.; Giannini, L.; Floriani, C.; Re, N.; Chiesi-Villa, A.; Rizzoli, C. *Inorg. Chim. Acta* **1998**, *270*, 298.

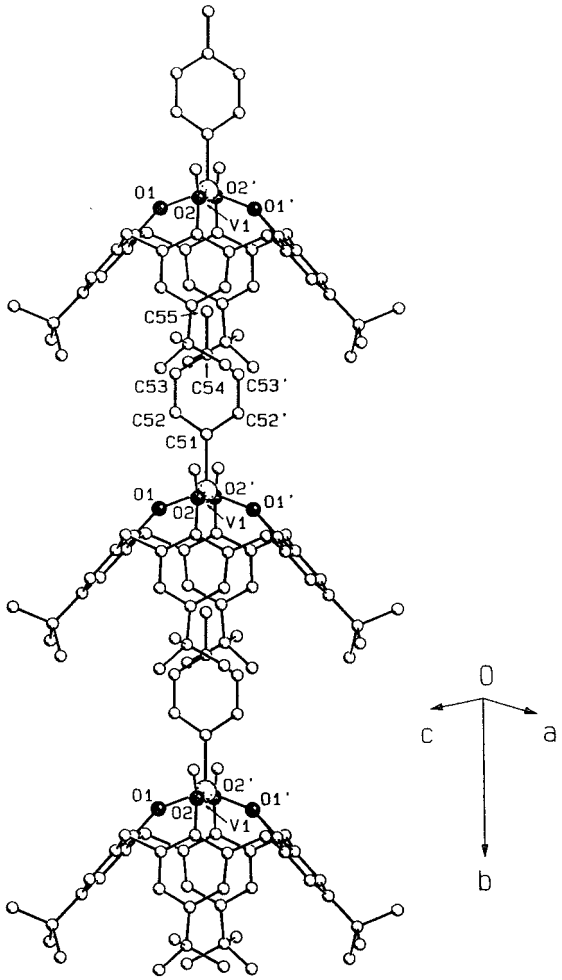

Figure 3. SCHAKAL view of complex **5** showing the chaining along the [010] axis. Disorder has been omitted for clarity. Prime denotes a transformation of $-x, y, 0.5 - z$.

(3.731(7)−3.864(9) Å) suggests the methyl protons point toward the centroid of the rings. The macrocycle assumes an elliptical cross section conformation elongated along the O1···O1′ direction, very close to that observed in complex **2**. The aromatic ring of the guest *p*-tolyl ligand is oriented nearly parallel to the O(1),V,O(1)′ direction (dihedral angle 5.1(2)°) and perpendicular to the C(1)···C(6) and C(1)′···C(6)′ rings (dihedral angle 86.5(2)°). The O_4 core shows a remarkable tetrahedral distortion (displacements ranging from −0.150(3) to 0.264(4) Å), with vanadium protruding by 0.381(1) Å from the mean plane. The coordination environment around vanadium can be described as a trigonal bipyramid, the equatorial plane being defined by the O(1), O(1)′, C(51), and V atoms, which are planar from symmetry requirements. O(2) and O(2)′ occupy the apexes (O(2)−V−O(2)′ 167.6(1)°). The distortion from an ideal trigonal symmetry is mainly indicated by the value of the O(1)−V−O(1)′ bond angle (139.0(2)°). The V−O(2) (2.137(4) Å) and V−O(1) (1.841(5) Å) bond

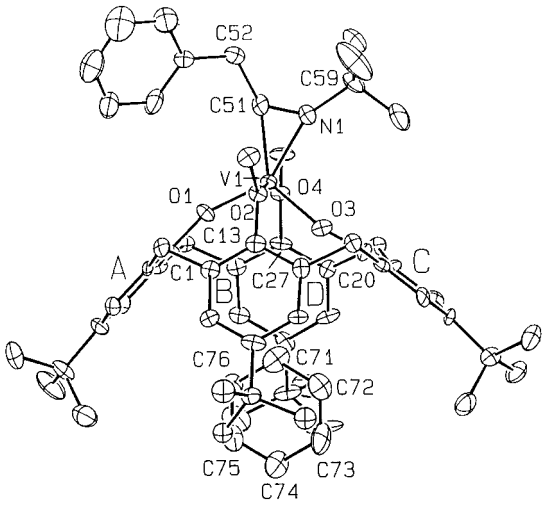

Figure 4. ORTEP drawing of complex **9** (50% probability ellipsoids). Disorder has been omitted for clarity.

distances parallel those observed in complex **2**, while the V−C(51) distance (2.042(10) Å) is in the usual range.[22]

The V−C bond in complexes **3**−**5** can be engaged in migratory insertion reactions both with carbon monoxide and Bu^{t}NC (Scheme 1). The reaction with CO is strongly dependent on the alkyl substituent. In the case of methyl and benzyl substituents, we were able to isolate the corresponding η^2-acyls, **6** and **7**. In the case of *p*-tolyl, the absorption of CO was limited and we were unable to identify a single characterizable compound. The η^2-bonding mode of the acyl group has been inferred from the absence in the IR spectrum of any CO band higher than 1600 cm^{-1} and by analogy with the corresponding η^2-iminoacyl compound (see below).[23] The reaction of **3**−**5** with Bu^{t}NC was carried out in benzene at room temperature and led (see Scheme 1) to the isolation of **8**−**10**. The IR spectra showed the C═N band of the η^2-iminoacyl in the 1614−1625 cm^{-1} region. The migratory insertion of alkyl and aryl groups to isocyanides in vanadium(III) chemistry has some significant precedents.[22,23]

The proposed structure for the η^2-iminoacyl functionality in **8**−**10** is supported by the X-ray analysis of **9** (see Figure 4). The O_4 core shows a remarkable tetrahedral distortion (displacements ranging from −0.379(5) to 0.366(5) Å), with vanadium protruding by 0.658(2) Å from the mean plane. The plane of the η^2-bonded atoms (V, N(1), C(51)) is perpendicular to the O_4 mean plane (dihedral angle 87.3(2)°). The V−O bond distances (V−O(2) 2.179(4) Å; V−O(4) 2.161(3) Å; V−O(1) 1.883(5) Å; V−O(3), 1.860(4) Å) are significantly longer than in **2** and **5**, while the approximate linearity of the V−O(1)−C(1) (159.9(4)°) and V−O(3)−C(20) (169.1(4)°) bond angles is maintained. The η^2-bonded N,C fragment shows a symmetric bonding mode to the metal (V−N(1) 2.050(7) Å; V−C(51) 2.047(8) Å) and a N(1)−C(51) distance of 1.266(8) Å.[22] The calixarene ligand assumes a conformation of elliptical cross section, similar to that observed in **2** and **5**, allowing the inclusion of a benzene molecule which enters the cavity nearly parallel to the O(1),V,O(3) plane (dihedral angle 5.6(2)°) and perpen-

(22) Vivanco, M.; Ruiz, J.; Floriani, C.; Chiesi-Villa, A.; Rizzoli, C. *Organometallics* **1993**, *12*, 1802 and 1794. Ruiz, J.; Vivanco, M.; Floriani, C.; Chiesi-Villa, A.; Rizzoli, C. *Organometallics* **1993**, *12*, 1811. Jacoby, D.; Floriani, C.; Chiesi-Villa, A.; Rizzoli, C. *J. Chem. Soc., Chem. Commun.* **1991**, 790. Rosset, J.-M.; Floriani, C.; Mazzanti, M.; Chiesi-Villa, A.; Guastini, C. *Inorg. Chem.* **1990**, *29*, 3991.

(23) Durfee, L. D.; Rothwell, I. P. *Chem. Rev.* **1988**, *88*, 1059 and references therein.

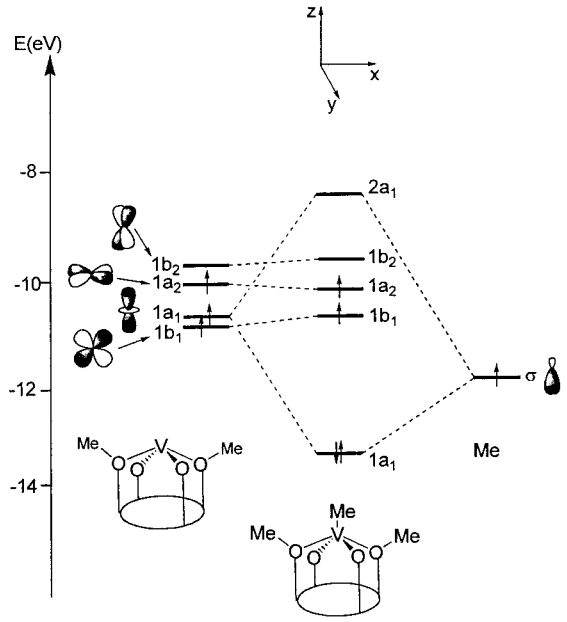

Figure 5. Interaction diagram for the valence orbitals of **3**.

dicular to the C(1)···C(6) and C(15)···C(20) rings (dihedral angles 87.0(2)° and 83.4(2)°, respectively) with the C(71)−H(71) bond directly below the vanadium atom (V···C(71) 4.692(9) Å; V···H(71)−C(71) 176.1°). In this orientation, the H(72) and H(76) atoms of the guest point toward the A and C rings, respectively, as indicated by the narrow range of the H(72)···$C_{ring\ C}$ and H(76)···$C_{ring\ A}$ contact distances, which vary from 2.95 to 3.06 Å and from 3.05 to 3.25 Å, respectively. At the same time, a CH_3/π host−guest interaction seems to take place involving the C(44) methyl group.[24] The contact distances involving the H(441) methyl hydrogen are in the range from 2.92 to 3.29 Å for the C(72)···C(75) group of atoms, while the H(441)−C(71) and H(441)−C(76) distances are greater than 3.5 Å.[21,24]

Extended Hückel calculations[25] have been performed on the calix[4]arene−vanadium derivatives with the purpose of understanding the frontier orbitals of the [calix[4]-$(OMe)_2(O)_2$V] fragment, the bonding of the organometallic functionalities in **3**−**10**, and the conversion of the V−alkyl and V−aryl bonds (**3**−**5**) into the corresponding η^2-acyl and iminoacyl derivatives (**6**−**10**).

The calix[4]arene ligand has been slightly simplified by replacing it with four phenoxo groups and symmetrizing to a C_{4v} geometry. This simplified model retains the main features of the whole ligand with the geometrical constraints on the O_4 set of donors atoms being maintained by fixing the geometry of the four phenoxo groups to the experimental X-ray values. Let us first consider complex **3**, in which the Me ligand lies along the *z* axis. The electronic structure is analyzed in terms of the interactions between the frontier orbitals of the [calix[4]$(OMe)_2(O)_2$V)] metal fragment and the Me moiety. The frontier orbitals of the [calix[4]$(OMe)_2(O)_2$V] fragment are shown on the left of Figure 5 and consist of four low-lying metal-based orbitals. We can distinguish two low-lying almost degenerate orbitals, i.e., $1b_1(d_{xz})$, pointing in the plane of the two methoxy ligands, and $1a_1(d_{z^2})$. Due to the stronger σ and π interactions with the phenoxo ligands in the *yz* plane, $1b_2(d_{yz})$ is almost 1 eV higher in energy than $1b_1(d_{xz})$. Due to the in-plane π interaction with the nonmethylated O atom, the $1a_2(d_{xy})$ orbital is destabilized and lies only 0.3 eV lower in energy. On the extreme right of Figure 5 is the singly occupied σ orbital of Me. Figure 5 shows that the main bonding interaction for this system is between $1a_1(d_{z^2})$ of the metal fragment and the σ orbital of CH_3. The remaining low-lying orbitals of the metal fragment remain essentially unaltered. It follows that for such a d^2 V(III) complex we would expect a triplet ground state with the closely spaced $1b_1(d_{xz})$ and $1a_2(d_{xy})$ orbitals singly occupied, which is in agreement with the observed magnetic behavior.

A similar situation is found in complex **2** for the π-donor ligand Cl^- where the interaction with the π donor orbitals of Cl^- leads to a destabilization of $1b_1(d_{xz})$ (the only orbital which does not show π interactions with O atoms) but not of $1a_2(d_{xy})$, which in turn inverts the order of the two singly occupied orbitals. Complex **2** reacts with Lewis bases, illustrated here by Bu^tNC, to give complex **11**, which has been characterized by elemental analysis, IR, and magnetism studies (see Experimental Section). The observed magnetic moment (μ_{eff} = 2.67 μ_B at 300 K) corresponds to a d^2 high-spin system and emphasizes the difference with the corresponding vanadium(III) [Cp_2V(X)(Y)] derivative (Cp = η^5-C_5H_5).[26] In the latter case, the metal is diamagnetic due to the availability of three orbitals at the metal only. In the case of **11**, the high-spin state is allowed with the availability of four orbitals at an accessible energy, with the two unpaired electrons in $1a_2$ and $1b_1$ (see Figure 6). Complex **11** can be considered as a model for the incoming inserting ligand preceding the insertion reaction. The migratory insertion reactions leading to **6**−**10** have been exemplified by the reaction of **3** with carbon monoxide. Since the extended Hückel method is not very well suited to describe the energetics of bond breaking and bond formation, we examined only the initial approach of CO to vanadium. The most favorable approach of the CO or Bu^tNC nucleophilic species is determined by the spatial extension of the $1b_1(d_{yz})$ LUMO. The attack is, therefore, expected to occur along a line in the *yz* plane forming an angle of approximately 45° with the *z* axis. We first simulated the initial stages of the CO attack by performing extended Hückel calculations on the [calix[4]$(OMe)_2(O)_2$VMe]−CO system with different (CO)-to-metal distances, from 5.0 to 2.5 Å, along a line in the *yz* plane by relaxing the axial position of the Me ligand and the angular position of CO to the *z* axis at each point along the attack pathway. The total energy profile is given in Figure 7 and shows a very small energy barrier followed by a significant stabilization, in harmony with the experimental evidence for a facile CO insertion. It is worth noting that for the shortest considered (CO)-to-metal distance there is a significant back-donation from the occupied vanadium $1b_1(d_{xz})$ orbitals to the π^* orbital of CO. This is confirmed by the fragment orbital populations calculated for V−CO = 2.5 Å which show a significant

(24) Andreetti, G. D.; Ugozzoli, F. In *Calixarenes, A Versabile Class of Macrocyclic Compounds*; Vicens, J., Böhmer, V., Eds.; Kluwer: Dordrecht, The Netherlands, 1991; pp 88−122.

(25) Hoffmann, R.; Lipscomb, W. N. *J. Chem. Phys.* **1962**, *36*, 2179. Hoffmann, R. *J. Chem. Phys.* **1963**, *39*, 1397.

(26) Poli, R. *Chem. Rev.* **1996**, *96*, 2135.

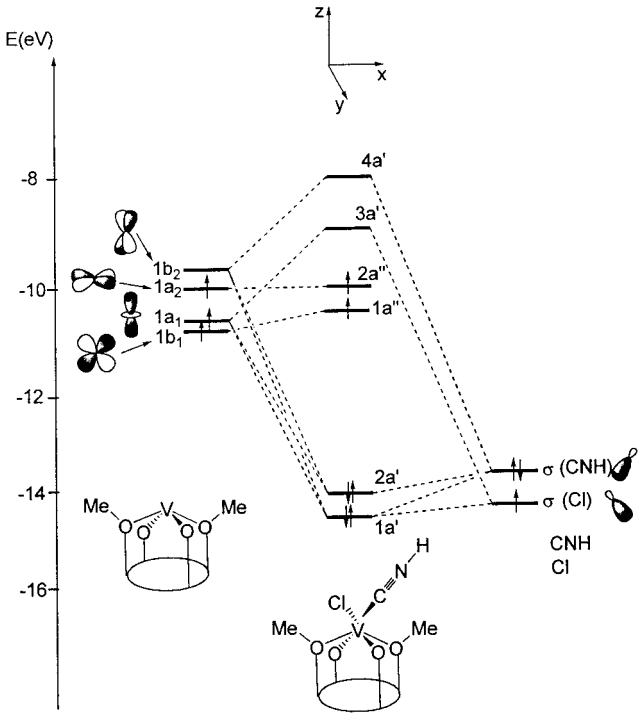

Figure 6. Interaction diagram for the valence orbitals of **2**.

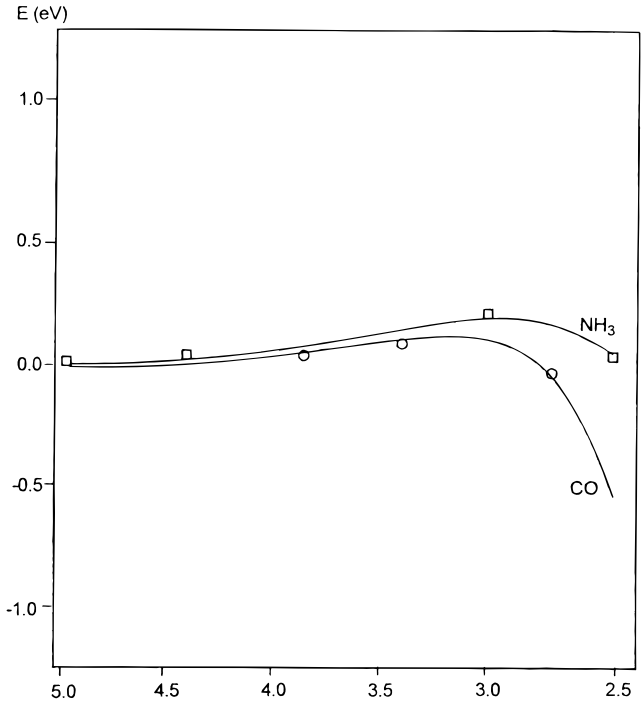

Figure 7. Total energy profiles for the CO (○) and NH_3 (□) approach toward **3**.

population of the π^* orbital of CO (0.21 vs 0.00 for isolated CO) and a simultaneous depopulation of the two singly occupied metal orbitals (1.77 vs 2.00 for the isolated fragment).

Let us now consider the η^2-acyl complex [calix[4]-$(OMe)_2(O)_2V(\eta^2$-COMe)]. The bonding between the metal fragment and the acyl moiety is illustrated by the interaction orbital diagram in Figure 8. The extreme right of Figure 8 shows the frontier orbitals of the acyl ligand, i.e., the HOMO n_-, consisting of the out-of-phase

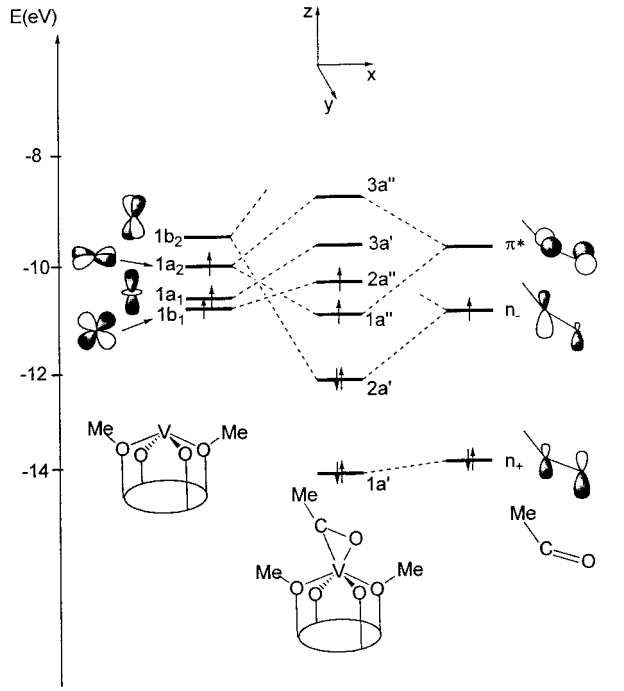

Figure 8. Interaction diagram for the valence orbitals of **6**.

combination of the carbon and the oxygen p_z orbitals, the lower lying n_+, which is the corresponding in-phase combination, and the CO π and π^* orbitals. We see that the vanadium acyl bonding is mainly achieved through the interaction between the metal d_{yz} and the acyl n_-, orbitals with minor σ, $d_{z^2}-n_+$, and δ, $d_{xy}-\pi^*$(CO) contributions (we considered an orientation with the acyl plane lying in the *yz* symmetry plane of the C_s molecule with the CO bond perpendicular to the *z* axis).

The vanadium(III) complexes so far mentioned display interesting redox behavior. Compounds **2** and **5** treated with 1 equiv of iodine led to the corresponding vanadium(IV) derivatives **12** and **13**, respectively. Both compounds have been analytically characterized, including magnetic moments, and show a d^1 configuration (**13** shows a $\mu_{eff} = 1.65\ \mu_B$ at 300 K); the corresponding hydrolysis product was [*p*-Bu^t-calix[4]-(OMe)$(OH)_3$]. The oxidation with I_2 is particularly remarkable in the reaction of **5** to **13** since the V−C bond is not affected by the oxidation process. The reaction occurs with the simultaneous loss of MeI (see Experimental Section). The MO diagram in Figure 5 suggests that the oxidation involves the removal of one electron from an essentially pure d orbital, that is $1a_2$. In the resulting vanadium(IV) cationic complex, the strong nucleophile I^- removes the methyl group from a methoxy substituent activated by the relatively high metal oxidation state. In several cases, we observed demethylation of the methoxy groups in the interaction of methoxy-calix[4]arenes with high-valent metals.[2h] The methoxy group not only functions as a weakly binding group, but it can also undergo an acid- or redox-assisted conversion into the corresponding anion. We should also emphasize the synthetic relevance of the reaction of **2** and **5** with iodine, since complexes **12** and **13** would be hardly accessible from a different route. In the case an excess of I_2 being used in the oxidation of **5** to **13**, the reaction proceeds further with the cleavage of the V−C bond and the complete

demethylation of calix[4]arene. The reaction may proceed via the intermediacy of the corresponding vanadium(IV) monoiodide derivative, which transfers I^- to the methyl of the residual methoxy group. Complex **14** has been obtained as a crystalline solid and structurally characterized.[27] All attempts to convert **6**−**10** to the corresponding vanadium(IV) derivatives via the iodine oxidation failed, at least partially, because the demethylation parallels the R−C cleavage in the η^2-acyls and η^2-iminoacyls.

Conclusions

Some relevant results from the present report should be emphasized:

(i) The synthesis and migratory insertion of V−C functionalities anchored exclusively to an oxo-matrix provided by the O_4 set from a calix[4]arene.

(ii) The oxidative demethylation of the methoxy-calix[4]arene, which converts vanadium(III) into vanadium(IV) organometallic functionalities, emphasizes the role of the methoxy group allowing interconversion between two oxidation states of the metal bearing the same functionality.

(iii) The magnetic properties of hexacoordinate d^2 high-spin vanadium(III) showed the availability of four frontier orbitals for the [*p*-Bu^t-calix[4]-$(OMe)_2(O)_2$V] fragment. This has been confirmed by the extended Hückel calculations and gives us a better picture of the bonding mode of the various organometallic functionalities and of the migratory insertion reactions.

(27) A preliminary X-ray analysis confirmed the structure proposed for **14**.

Acknowledgment. We thank the Fonds National Suisse de la Recherche Scientifique (Bern, Switzerland, Grant No. 20-46′590.96), Ciba Specialty Chemicals (Basle, Switzerland), and Fondation Herbette (University of Lausanne, N. Re) for financial support.

Supporting Information Available: SCHAKAL drawings and tables of crystal data, atomic coordinates, thermal parameters, and bond distances and angles for **2**, **5**, and **9** (19 pages). Ordering information is given on any current masthead page.

OM9800389